

Cite this: *J. Mater. Chem. C*, 2022,  
10, 2711

## Facile synthesis, precise species control and chemical transformation of highly conducting organic metal chalcogenides $\text{Cu}_x\text{BHT}$ (BHT = benzenehexathiol; $x = 3, 4, \text{ and } 5.5$ )<sup>†</sup>

Yigang Jin,<sup>ab</sup> Yang Li,<sup>ab</sup> Yong Sun,<sup>ab</sup> Mengsu Zhu,<sup>ab</sup> Ze Li,<sup>ab</sup> Liyao Liu,<sup>ab</sup> Ye Zou,<sup>ab</sup> CaiMing Liu,<sup>id</sup> Yimeng Sun<sup>ab</sup> and Wei Xu<sup>id</sup>\*<sup>ab</sup>

The design of conducting organic metal chalcogenides (OMCs) has attracted extensive attention for their applications in diverse areas. However, only a handful of OMCs exhibit appealing electrical transport properties due to the limited synthetic approaches. Herein, a facile and controllable synthetic approach for the preparation of highly crystalline benzenehexathiol (BHT)-based OMCs using  $\text{Cu}_2\text{O}$  as a precursor is reported. Under heterogeneous conditions, a series of highly conducting organic metal chalcogenides  $\text{Cu}_x\text{BHT}$  ( $x = 3, 4, \text{ and } 5.5$ ) were precisely constructed *via* variation of the molar ratio between  $\text{Cu}_2\text{O}$  and BHT. In particular, a fascinating chemical transformation phenomenon was discovered in this work. This is the first time that a phase transition has been observed in conducting OMCs, with the semiconducting species ( $\text{Cu}_4\text{BHT}$  and  $\text{Cu}_{5.5}\text{BHT}$ ) being converted to metallic species ( $\text{Cu}_3\text{BHT}$ ) under delicate oxidation regulation. This work provides a prominent paradigm for constructing highly crystalline OMCs, and opens up the possibility of developing OMCs with different structural topologies through chemical transformation.

Received 3rd August 2021,  
Accepted 20th September 2021

DOI: 10.1039/d1tc03614a

rsc.li/materials-c

## Introduction

Organic metal chalcogenides (OMCs) refer to a class of hybrid materials containing continuous M–X ( $X = \text{S, Se, Te}$ ) networks and organic units covalently linked *via* chalcogen atoms.<sup>1,2</sup> Owing to their highly tunable electronic structures and electrical transport properties, OMCs have received extensive attention in recent years.<sup>3,4</sup> Based on their chemical and electronic structures, OMCs can be divided into two subclasses. The first type of OMCs has one-dimensional (1D) and two-dimensional (2D) organic units separated by inorganic cores, and there is weak electronic coupling between the inorganic and organic subunits. This species is the most reported one, which is usually constructed with ligands bearing only one chalcogen coordination group.<sup>5–7</sup> Due to their 1D or 2D core–shell structures, highly anisotropic transport properties could be expected which leads to relatively inferior performance. This is especially evident for OMCs obtained as polycrystalline samples.<sup>8</sup> This situation has changed obviously with the emergence of the 2nd

generation OMCs constructed from benzenehexathiol (BHT), which display strong electronic coupling among the inorganic subunits as well as between the organic and inorganic subunits, while the organic units (conjugated molecular systems) are embedded in the inorganic networks. Apart from the commonly observed 2D honeycomb lattice containing discrete  $\text{MS}_4$  subunits separated by benzene rings,<sup>9,10</sup> BHT displays great flexibility in constructing coordination polymers with different structural topologies. From the early reported  $\text{Pb}_3\text{BHT}$ <sup>11</sup> to the later  $\text{Ag}_5\text{BHT}$ <sup>12</sup> and  $\text{Cu}_x\text{BHT}$  ( $x = 3, 4, \text{ and } 5.5$ ),<sup>13,14</sup> all these materials are OMCs with 2D or complex 3D M–S networks.

Compared with the 1st generation OMCs, BHT-based 2nd generation OMCs display superior electrical transport properties,<sup>15</sup> as well as great potential for electrochemical catalysts,<sup>10,16</sup> transparent electrodes<sup>17</sup> and energy storage devices.<sup>18,19</sup> Moreover, exotic quantum phenomena have been observed in  $\text{Cu}_3\text{BHT}$  such as unconventional superconductivity and quantum spin liquid (QSL) behaviour.<sup>20,21</sup> All these characteristics make these BHT-based OMCs extremely attractive especially the  $\text{Cu}_x\text{BHT}$  family. However, the synthetic methods that are crucial for crystallinity and phase purity control are less investigated. For  $\text{Cu}_4\text{BHT}$  and  $\text{Cu}_{5.5}\text{BHT}$ , it is supposed that unintentional oxidation of the ligand plays a critical role in the resulting species control according to their nonstoichiometric composition.<sup>13</sup> But it remains a highly tricky process for the

<sup>a</sup> Beijing National Laboratory for Molecular Sciences, Key Laboratory of Organic Solids, Institute of Chemistry, Chinese Academy of Sciences, Beijing 100190, China. E-mail: wxu@iccas.ac.cn

<sup>b</sup> University of Chinese Academy of Sciences, Beijing 100049, China

<sup>†</sup> Electronic supplementary information (ESI) available. See DOI: 10.1039/d1tc03614a

synthesis of  $\text{Cu}_{5.5}\text{BHT}$  with sufficient phase purity through a homogeneous reaction. In addition, the tendency of  $\text{Cu}_{5.5}\text{BHT}$  converting to  $\text{Cu}_4\text{BHT}$  and even to  $\text{Cu}_3\text{BHT}$  has been observed with the reaction prolonged. But how to achieve a controllable transformation among these  $\text{Cu}_x\text{BHT}$  members is still elusive. The solution to this conundrum will offer an alternative synthesis strategy for these OMCs and will provide valuable information about the chemical state of building units in the polymers.

Herein, we successfully obtained all members of the  $\text{Cu}_x\text{BHT}$  ( $x = 3, 4, \text{ and } 5.5$ ) family through a facile heterogeneous reaction using  $\text{Cu}_2\text{O}$  as the copper source. The identity and phase purity of the resulting OMCs can be easily controlled by modulating the molar ratio of  $\text{Cu}_2\text{O}$  and BHT. Furthermore, we discovered that the chemical transformation can be realized within the  $\text{Cu}_x\text{BHT}$  family by using tris(4-bromophenyl)aminium hexachloroantimonate ( $((4\text{-BrPh})_3\text{NSbCl}_6)$ ) as the oxidizing reagent. Under precise oxidation regulation with  $(4\text{-BrPh})_3\text{NSbCl}_6$ ,  $\text{Cu}_{5.5}\text{BHT}$  can be converted to  $\text{Cu}_4\text{BHT}$ , and even to  $\text{Cu}_3\text{BHT}$  under further oxidation. This is the first time that such fascinating chemical transformation among the semiconducting OMCs ( $\text{Cu}_{5.5}\text{BHT}$  to  $\text{Cu}_4\text{BHT}$ ), semiconducting to metallic OMCs ( $\text{Cu}_{5.5}\text{BHT}$ ,  $\text{Cu}_4\text{BHT}$  to  $\text{Cu}_3\text{BHT}$ ), has been observed. These results provide a simple and controllable strategy for the synthesis of highly crystalline OMCs, and highlight the significance of chemical structure regulation as well as the electronic structure modulation of OMCs by a chemical method.

## Results and discussion

### Synthesis and characterization

As schemed in Fig. 1,  $\text{Cu}_x\text{BHT}$  series were prepared at  $80^\circ\text{C}$  by modulating appropriate stoichiometric ratios between  $\text{Cu}_2\text{O}$

and BHT. Under an argon atmosphere, when 1.5 equivalents of  $\text{Cu}_2\text{O}$  (23.6 mg, 0.165 mmol) and BHT (30 mg, 0.11 mmol) were mixed in 30 mL of degassed ethanol and reacted for 72 h, a black  $\text{Cu}_3\text{BHT}$  sample was obtained. Similarly, when 2 equivalents of  $\text{Cu}_2\text{O}$  (31.5 mg, 0.22 mmol) and BHT (30 mg, 0.11 mmol) reacted for 48 h in 30 mL of degassed ethanol, a dark blue  $\text{Cu}_4\text{BHT}$  was obtained. When 2.75 equivalents of  $\text{Cu}_2\text{O}$  (43.3 mg, 0.303 mmol) and BHT (30 mg, 0.11 mmol) reacted for 48 h in 30 mL of degassed acetonitrile, a dark green  $\text{Cu}_{5.5}\text{BHT}$  was obtained. The strong signal at  $\sim 2490\text{ cm}^{-1}$  that can be ascribed to the S–H stretching vibration in BHT disappeared (Fig. S1, ESI<sup>†</sup>), indicating that all the thiol groups of BHT participated in the reaction with  $\text{Cu}_2\text{O}$ . Besides, powder X-ray diffraction (PXRD), elemental analysis (EA), and inductively coupled plasma (ICP) were performed to confirm that the attained samples had the same components and structures as previously reported (Fig. S2–S4, see the ESI<sup>†</sup>).<sup>13,20</sup> The self-assembly coordination and reaction kinetics between  $\text{Cu}_2\text{O}$  and thiolate species are quite unique.<sup>8,22,23</sup> We have observed that  $\text{Cu}_3\text{BHT}$  can also be obtained by a long-term reaction of 1.5 equivalents of  $\text{Cu}_2\text{O}$  with BHT, which is quite different from the previously reported  $\text{CuCl}_2$  (Fig. 1).<sup>16</sup> Recent magnetic susceptibility measurements<sup>20</sup> in  $\text{Cu}_3\text{BHT}$  unveiled that the oxidation state of Cu is +2, and thus we infer that the  $\text{Cu}^+$  source is oxidized to  $\text{Cu}^{2+}$  gradually during the reaction process.

Typically, PXRD data were collected to investigate the crystallinity of the obtained samples. As evidenced by sharp, well-isolated diffraction peaks, the crystallinity of  $\text{Cu}_3\text{BHT}$  is much higher than that of the products obtained with  $\text{Cu}^{2+}$  salts as reactants (Fig. S2, ESI<sup>†</sup>). Meanwhile, the morphologies of  $\text{Cu}_x\text{BHT}$  ( $x = 3, 4, \text{ and } 5.5$ ) were characterized by scanning electron microscopy (SEM) and transmission electron microscopy (TEM)

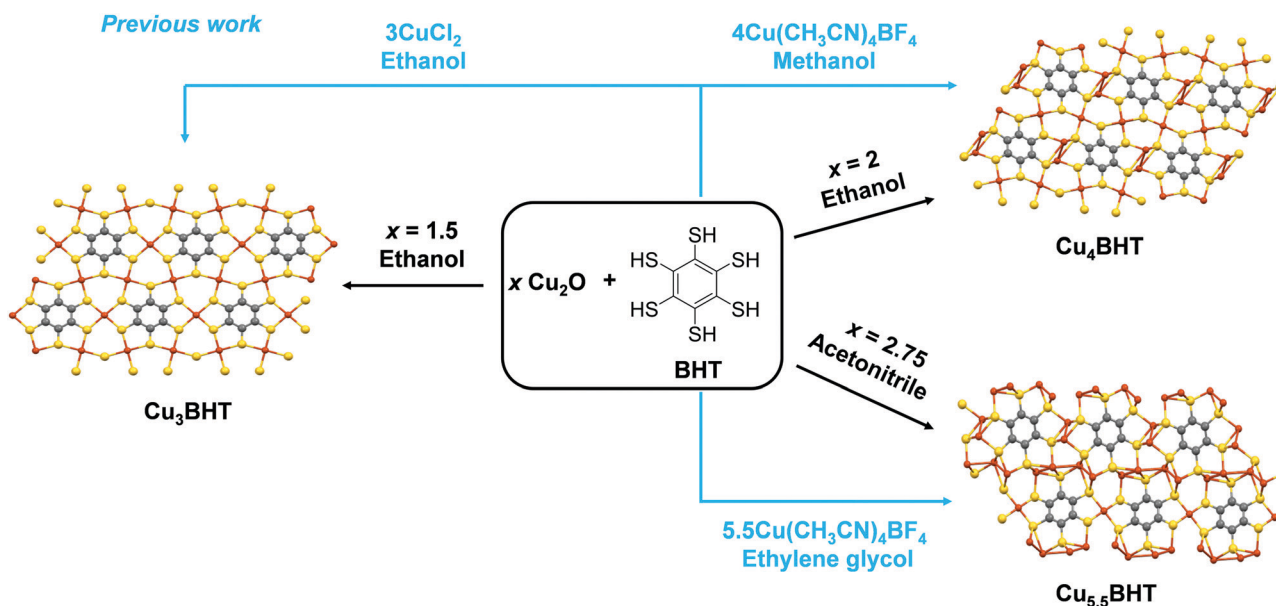


Fig. 1 Comparison of the synthetic methods of  $\text{Cu}_x\text{BHT}$  ( $x = 3, 4, \text{ and } 5.5$ ). The schematic synthesis of  $\text{Cu}_x\text{BHT}$  using different metal sources and reaction solvents. The previously reported pathways (ref. 13 and 16) are indicated by blue lines and text.

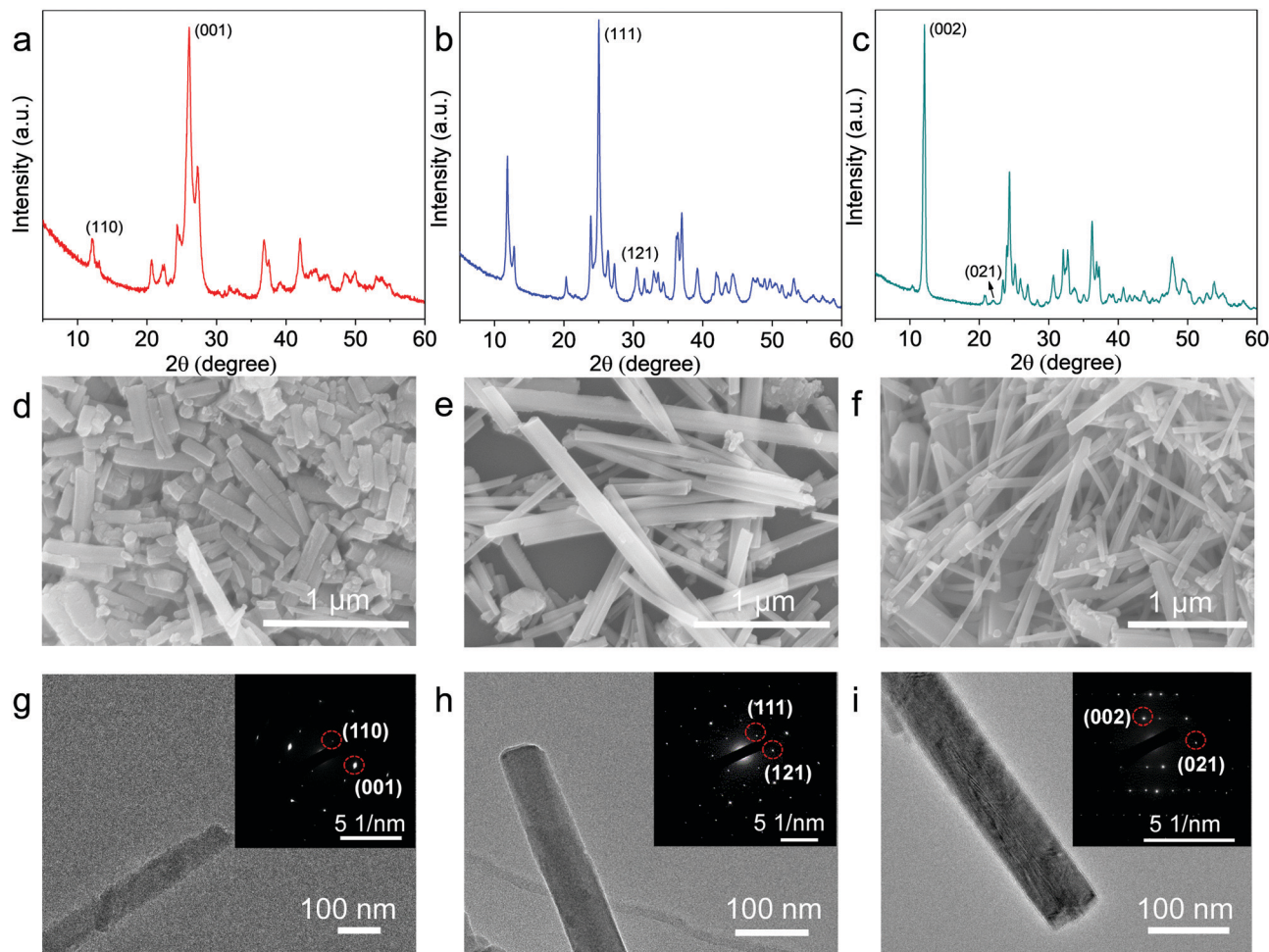


Fig. 2 Characterization of  $\text{Cu}_x\text{BHT}$ . (a–c) PXRD patterns of  $\text{Cu}_3\text{BHT}$ ,  $\text{Cu}_4\text{BHT}$  and  $\text{Cu}_{5.5}\text{BHT}$ , respectively. (d–f) SEM images of  $\text{Cu}_3\text{BHT}$ ,  $\text{Cu}_4\text{BHT}$  and  $\text{Cu}_{5.5}\text{BHT}$ , respectively. (g–i) TEM images of  $\text{Cu}_3\text{BHT}$ ,  $\text{Cu}_4\text{BHT}$  and  $\text{Cu}_{5.5}\text{BHT}$ , respectively. Insets correspond to SAED patterns.

(Fig. 2). As indicated in the SEM images, all three samples displayed regular rod-like structures with a smooth surface and uniform size. The as-prepared nanorods are a few tens of nanometers in diameter and range from 500 nm ( $\text{Cu}_3\text{BHT}$ ) to 2 μm ( $\text{Cu}_4\text{BHT}$  and  $\text{Cu}_{5.5}\text{BHT}$ ) in length (Fig. 2d–f), which are longer than the nanocrystals prepared with  $\text{Cu}^{2+}$  and  $[\text{Cu}(\text{CH}_3\text{CN})_4]\text{BF}_4$  salts.<sup>13,16</sup> In particular, the selected area electron diffraction (SAED) pattern of an individual nanorod revealed regularly spaced arrays of diffraction spots, which can be assigned very well to the respective crystal indices, as shown in Fig. 2g–i. All the PXRD, SEM and SAED results verified that the samples prepared with  $\text{Cu}_2\text{O}$  as precursors are highly crystalline OMCs, which are expected to be applied in microelectronic devices based on nano-crystalline materials. The improved crystallinity can be attributed to three aspects. First, it is believed that temperature is a crucial parameter during the growth process of OMCs. Generally, higher temperatures will improve the crystallinity of the resulting materials as the coordination bonding is more reversible, and defects can be healed during the crystal growth process. Second, the slow nucleation and growth process are critically important to obtain highly crystalline OMCs. Compared to common  $\text{Cu}^{2+}$  sources,

$\text{Cu}(\text{i})$  salts have a moderate reaction rate with organothiolates due to their more complicated  $d^{10}$  chemistry.<sup>24,25</sup> Furthermore, BHT and  $\text{Cu}_2\text{O}$  have poor solubility in reaction solvents, which reduces the reaction concentration and diffusion rate of precursors, thus resulting in improved crystallinity.

### Charge transport properties of $\text{Cu}_x\text{BHT}$

Electrical property characterization will provide further evidence on the identity of these  $\text{Cu}_x\text{BHT}$ s. To investigate the charge transport properties of these OMCs, the variable-temperature conductivities of the pressed pellets of  $\text{Cu}_x\text{BHT}$  were analysed using a standard four-probe method. As shown in Fig. 3, the conductivities of all the  $\text{Cu}_x\text{BHT}$  samples are compared with the previously reported results and are significantly higher than those of the most reported OMCs,<sup>8,15,19,26</sup> thus rendering them promising potential for applications in the microelectronics industry.<sup>27,28</sup> Among these three OMCs,  $\text{Cu}_3\text{BHT}$  features the highest electrical conductivity (215 to 286  $\text{S cm}^{-1}$  with an average value of 244  $\text{S cm}^{-1}$ ) compared with those of  $\text{Cu}_4\text{BHT}$  (153 to 184  $\text{S cm}^{-1}$  with an average value of 170  $\text{S cm}^{-1}$ ) and  $\text{Cu}_{5.5}\text{BHT}$  (144–166  $\text{S cm}^{-1}$  with an average value of 155  $\text{S cm}^{-1}$ ). According to



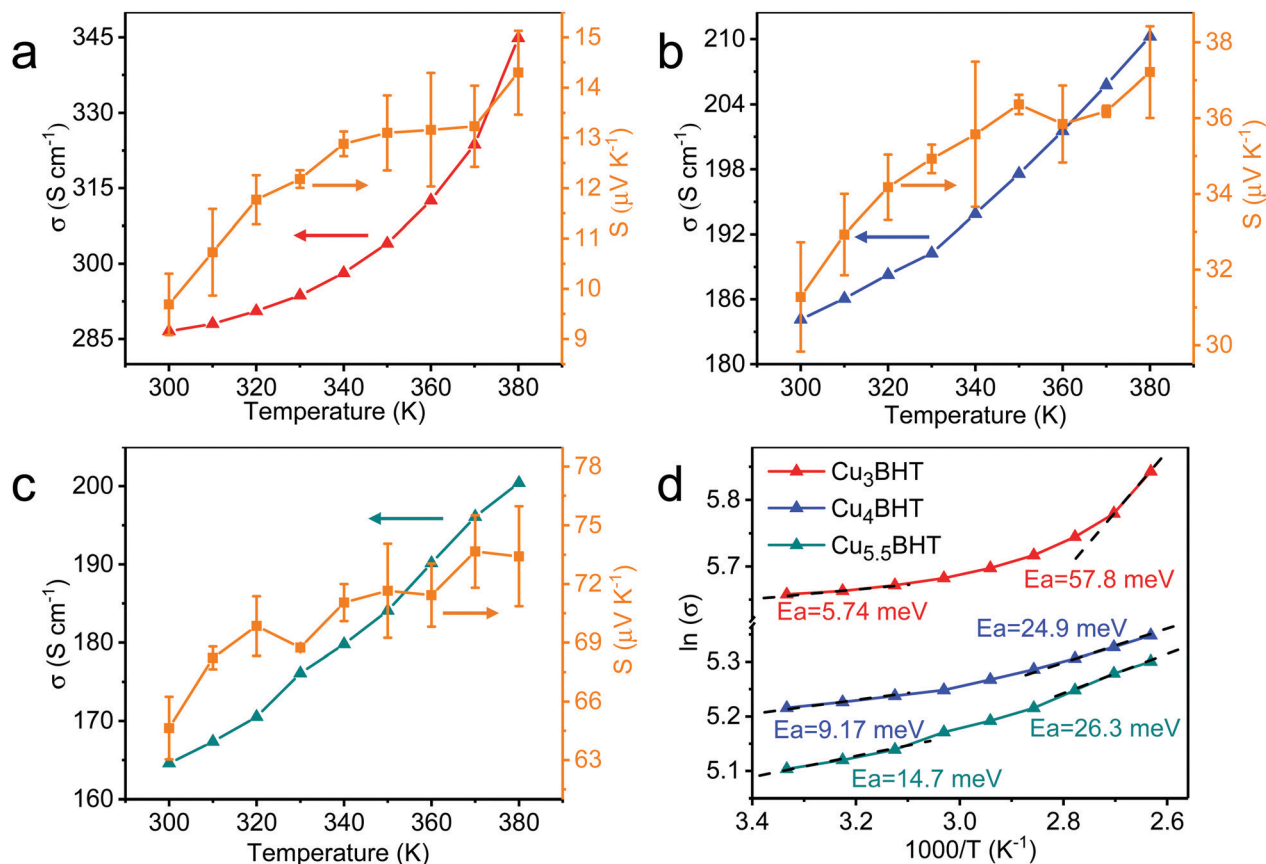


Fig. 3 The charge transport properties of Cu<sub>x</sub>BHT. (a–c) Curves of the variable-temperature electrical conductivity and Seebeck coefficient of Cu<sub>3</sub>BHT, Cu<sub>4</sub>BHT and Cu<sub>5.5</sub>BHT, respectively. (d) Plots of  $\ln(\sigma T)$  versus  $1000/T$  of Cu<sub>x</sub>BHT.

Arrhenius fitting, the plots of  $\ln(\sigma T)$  versus the reciprocal of the temperature give the activation energy ( $E_a$ ) of each sample (Fig. 3d). The  $E_a$  values for the electron hopping of these three OMCs at 300 K are in the sequence of Cu<sub>3</sub>BHT (5.74 meV) < Cu<sub>4</sub>BHT (9.17 meV) < Cu<sub>5.5</sub>BHT (14.7 meV), which explains the fact that the conductivities of Cu<sub>x</sub>BHT members are in the sequence of Cu<sub>3</sub>BHT > Cu<sub>4</sub>BHT > Cu<sub>5.5</sub>BHT. With the temperature increasing from 300 K to 380 K, the  $E_a$  of all three OMCs continuously increases, which indicates the defects, most likely the grain boundaries between neighbouring Cu<sub>x</sub>BHT nanocrystals that influence the charge transport behaviour.

It is obvious that the  $E_a$  of three OMCs appears quite small, especially in low temperature ranges. To figure out the origin of low  $E_a$  and observed high conductivities, three samples were subjected to ultraviolet photoelectron spectroscopy (UPS).

As illustrated in Fig. 4, all three samples displayed a clear Fermi edge near the top of the valence band, indicating that they are metallic conductors or degenerate semiconductors. As disclosed by band structure calculations, three networks exhibit substantial differences in their electronic structures. Cu<sub>3</sub>BHT has a metallic nature,<sup>20,21</sup> while Cu<sub>4</sub>BHT and Cu<sub>5.5</sub>BHT behave as degenerate semiconductors.<sup>13</sup> The differences in structural topology as well as the variation of hybridization between the d orbitals of the Cu ions and the  $\pi$  orbitals of the BHT ligands result in different band structures in the Cu<sub>x</sub>BHT family.

In addition, the variable-temperature Seebeck coefficient measurement displays that Cu<sub>3</sub>BHT has a small Seebeck coefficient ranging from 9 to 15  $\mu\text{V K}^{-1}$  (Fig. 3a–c). Such a low Seebeck coefficient and the weak temperature dependence of conductivity in Cu<sub>3</sub>BHT are typically observed in metals or highly conducting polymers,<sup>29</sup> which further demonstrates its metallic characteristic. In comparison, the Seebeck coefficients of Cu<sub>4</sub>BHT and Cu<sub>5.5</sub>BHT are 30–40  $\mu\text{V K}^{-1}$  and 60–80  $\mu\text{V K}^{-1}$ , respectively, which are about 3–6 times larger than that of Cu<sub>3</sub>BHT. The higher Seebeck coefficients suggest that Cu<sub>4</sub>BHT and Cu<sub>5.5</sub>BHT are more like degenerate semiconductors rather than metals, which is consistent with band structure calculation results.<sup>13</sup>

#### Oxidation regulation within the Cu<sub>x</sub>BHT family

Enlightened by the knowledge that redox has a significant influence on the oxidation states of metal bis(dithiolene) species and their electrical transport properties,<sup>12</sup> here, valence-variable (4-BrPh)<sub>3</sub>NSbCl<sub>6</sub> is employed as the oxidizing reagent since it is known to better control the oxidation states of the metal bis(dithiolene) unit.<sup>15,30,31</sup> In order to investigate the influence of the degree of oxidation on the final phases, different equivalents of (4-BrPh)<sub>3</sub>NSbCl<sub>6</sub> were added to Cu<sub>4</sub>BHT and Cu<sub>5.5</sub>BHT using methanol as a reaction medium. After post-preparation modification, the crystallinity and composition of the oxidation products were identified by PXRD, EA and ICP measurements

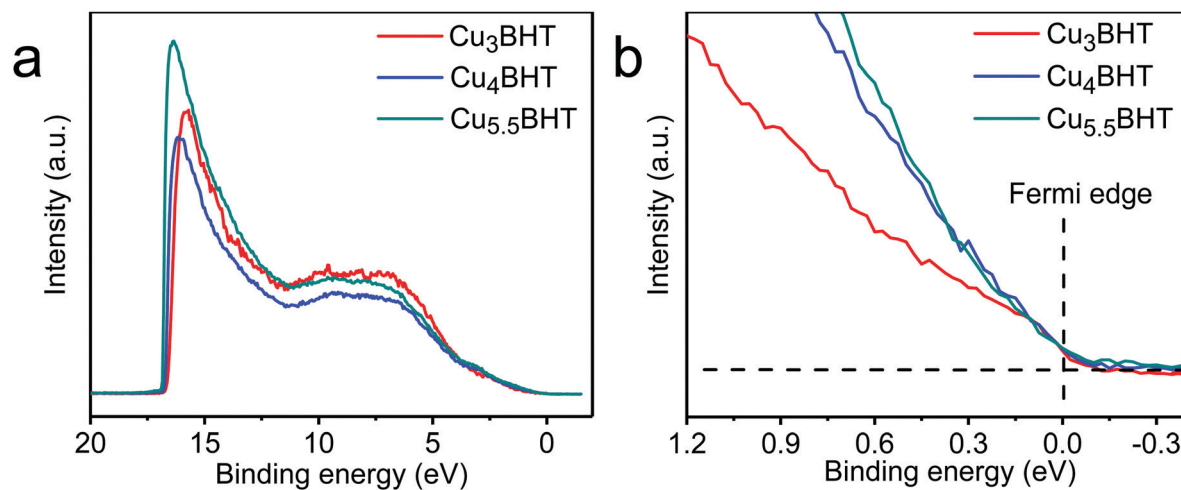


Fig. 4 The UPS analysis of  $\text{Cu}_x\text{BHT}$  acquired at 300 K. The full spectra and the Fermi edge are shown in (a) and (b), respectively.

(see Fig. S5 and S6, ESI<sup>†</sup>). Surprisingly, under an argon atmosphere, when 1.5 equivalents of  $(4\text{-BrPh})_3\text{NSbCl}_6$  (29.4 mg, 0.036 mmol) were added to  $\text{Cu}_{5.5}\text{BHT}$  (15 mg, 0.024 mmol) in 25 mL of  $\text{CH}_3\text{OH}$ , a dark blue  $\text{Cu}_4\text{BHT}$  sample was obtained at room temperature. When 2.5 equivalents of  $(4\text{-BrPh})_3\text{NSbCl}_6$  (49 mg, 0.06 mmol) were added to  $\text{Cu}_{5.5}\text{BHT}$  (15 mg, 0.024 mmol) or 1 equivalent of  $(4\text{-BrPh})_3\text{NSbCl}_6$  (24 mg, 0.029 mmol) was added to  $\text{Cu}_4\text{BHT}$  (15 mg, 0.029 mmol), a black  $\text{Cu}_3\text{BHT}$  sample was obtained (Fig. 5 and Fig. S2, ESI<sup>†</sup>). Such oxidation regulation accompanied by the changes in topological structures is quite rare among the other coordination polymers ever reported.<sup>32–35</sup> In addition, with the deepening oxidation degree, the colours of polycrystalline samples become gradually darker, varying from dark green, dark blue to black (Fig. 5). The visible difference in colours suggested that

$\text{Cu}_x\text{BHT}$  series have potential as light-harvesting or electrochromic materials.

During oxidation, the  $\text{Cu}$ – $\text{BHT}$  networks lose electrons and trigger structural conversions, and the entire system remains electrically neutral. After oxidation, the elemental composition of the oxidized products was analysed by X-ray photoelectron spectroscopy (XPS) (Fig. S7, ESI<sup>†</sup>). The  $\text{Cu}$  (2p) region exhibited a strong satellite peak, suggesting that the valence state of  $\text{Cu}$  in the remaining filtrate is +2. In the high-resolution  $\text{Sb}$  3d XPS spectrum, two sets of peaks with binding energies of  $\sim 540.4$  and  $\sim 531.1$  eV were observed and assigned, respectively, to the  $3d_{3/2}$  and  $3d_{5/2}$  levels of  $\text{Sb}$ , revealing that  $[\text{SbCl}_6]^-$  was reduced to  $[\text{SbCl}_6]^{3-}$ . On the basis of the charge balance, when  $\text{Cu}_{5.5}\text{BHT}$  loses 3 electrons,  $\text{Cu}_4\text{BHT}$  was generated, while  $\text{Cu}_3\text{BHT}$  was obtained when it loses 5 electrons. Similarly,  $\text{Cu}_4\text{BHT}$  can

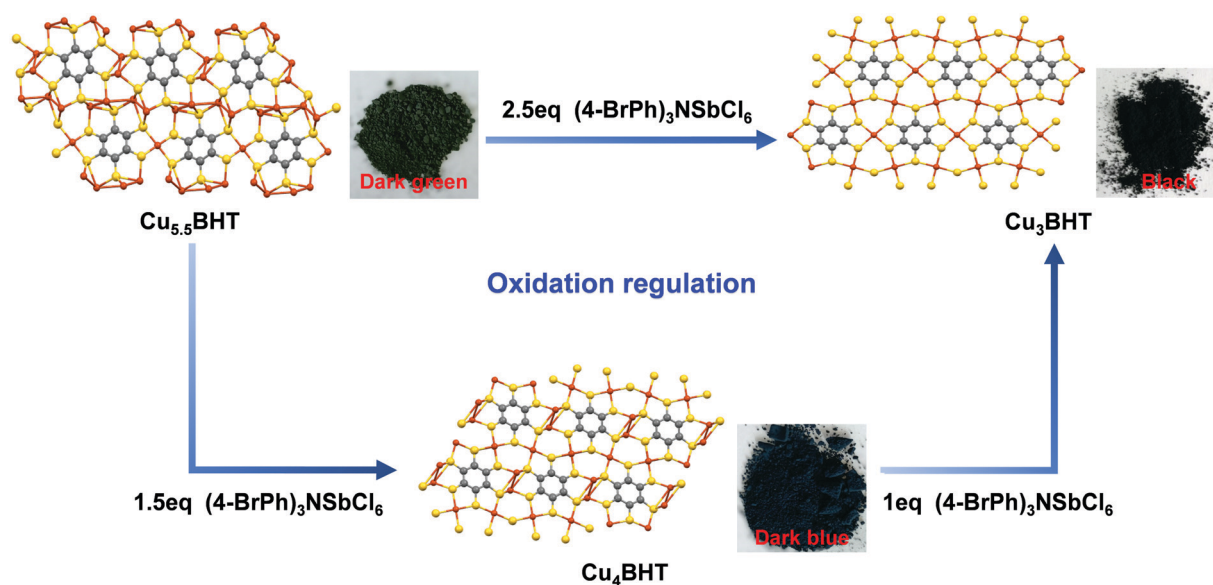


Fig. 5 Oxidation regulation within the  $\text{Cu}_x\text{BHT}$  family. Schematic illustration of phase transition in  $\text{Cu}_x\text{BHT}$  species upon delicate oxidation regulation with  $(4\text{-BrPh})_3\text{NSbCl}_6$ . Photograph shows the colours of each  $\text{Cu}_x\text{BHT}$  species.

transform into  $\text{Cu}_3\text{BHT}$  after losing 2 electrons, so  $\text{Cu}_4\text{BHT}$  is more like an intermediate state of transition from  $\text{Cu}_{5.5}\text{BHT}$  to  $\text{Cu}_3\text{BHT}$ . But it is a controversial issue to give a clear definition of whether the oxidation process is metal-centred or ligand-centred. We can infer that the copper bis(dithiolene) coordination unit, as an indivisible moiety, acts as an electron reservoir that can undergo complex redox switching as a whole. Thus, the ligand and the metal here cooperate in a synergistic manner, and their interplay facilitates the redox switching process. Therefore, the uniqueness of the oxidation states of BHT and the flexibility of the coordination geometries of  $\text{Cu}(I)$  ions result in rich members in the  $\text{Cu}_x\text{BHT}$  family. Additionally,  $\text{Cu}_{5.5}\text{BHT}$  and  $\text{Cu}_4\text{BHT}$  can be regarded as the reaction precursors of  $\text{Cu}_3\text{BHT}$  employing valence-variable  $[\text{SbCl}_6]^-$  as an oxidant. With this in mind, we hypothesized that the structural transformation induced by oxidation could be a promising synthetic shortcut to prepare the desired OMCs. Since the structural transformations in the  $\text{Cu}_x\text{BHT}$  family are accompanied by the changes in the optical, electrical and magnetic properties, they are expected to be employed for advanced functional applications such as sensors or electrochromic devices.

## Conclusions

In summary, three highly conducting OMCs –  $\text{Cu}_3\text{BHT}$ ,  $\text{Cu}_4\text{BHT}$  and  $\text{Cu}_{5.5}\text{BHT}$  – have been effectively prepared and characterized. By modulating the suitable feed ratios between  $\text{Cu}_2\text{O}$  and BHT, a series of  $\text{Cu}_x\text{BHT}$  ( $x = 3, 4, \text{ and } 5.5$ ) materials can be precisely generated, which has been evidenced by the combined analysis of EA, PXRD, SEM and SAED measurements. Here, the binary oxide  $\text{Cu}_2\text{O}$  as a metal source not only exhibits rich coordination capacity in constructing OMCs with different structural topologies, but also possesses moderate thiophilicity towards BHT, thereby obtaining a series of highly crystalline OMCs. It is particularly noteworthy that this synthetic pathway is facile and straightforward yet allows precise phase purity control. This discovery provides the possibility of producing new types of highly conducting OMCs. Most importantly, we demonstrate for the first time that the fantastic chemical transformation within the  $\text{Cu}_x\text{BHT}$  family can be realized under delicate oxidation regulation, in which both the semiconducting  $\text{Cu}_{5.5}\text{BHT}$  and  $\text{Cu}_4\text{BHT}$  can be converted to metallic  $\text{Cu}_3\text{BHT}$ . This interesting phenomenon highlights the importance of structural transformation for the control of electronic structures of OMCs. Considering the tailorable chemical structures and excellent performance of  $\text{Cu}_x\text{BHT}$  species, we believe that these OMCs have substantial potential for applications in the future.

## Conflicts of interest

There are no conflicts to declare.

## Acknowledgements

The authors acknowledge the financial support from the National Key R&D Program of China (Grant No. 2017YFA0204701),

the National Natural Science Foundation of China (Grant 22071256), and the Chinese Academy of Sciences (QYZDY-SSW-SLH024).

## Notes and references

- W. P. Su, M. C. Hong, J. B. Weng, Y. C. Liang, Y. J. Zhao, R. Cao, Z. Y. Zhou and A. S. C. Chan, *Inorg. Chim. Acta*, 2002, **331**, 8–15.
- H. Yan, J. N. Hohman, F. H. Li, C. Jia, D. Solis-Ibarra, B. Wu, J. E. P. Dahl, R. M. K. Carlson, B. A. Tkachenko, A. A. Fokin, P. R. Schreiner, A. Vaillonis, T. R. Kim, T. P. Devereaux, Z.-X. Shen and N. A. Melosh, *Nat. Mater.*, 2017, **16**, 349–355.
- O. Veselska and A. Demessence, *Coord. Chem. Rev.*, 2018, **355**, 240–270.
- Y. Li, X. Jiang, Z. Fu, Q. Huang, G.-E. Wang, W.-H. Deng, C. Wang, Z. Li, W. Yin, B. Chen and G. Xu, *Nat. Commun.*, 2020, **11**, 261.
- D. V. P. Massote and M. S. C. Mazzoni, *Appl. Phys. Lett.*, 2016, **109**, 133104.
- Y. Zhang, T. Xia, K. M. Yu, F. Zhang, H. Yang, B. Liu, Y. An, Y. Yin and X. Chen, *ChemPlusChem*, 2014, **79**, 559–563.
- C. Lavenn, N. Guillou, M. Monge, D. Podbevsek, G. Ledoux, A. Fateeva and A. Demessence, *Chem. Commun.*, 2016, **52**, 9063–9066.
- K. H. Low, V. A. Roy, S. S. Chui, S. L. Chan and C. M. Che, *Chem. Commun.*, 2010, **46**, 7328–7330.
- T. Kambe, R. Sakamoto, K. Hoshiko, K. Takada, M. Miyachi, J. H. Ryu, S. Sasaki, J. Kim, K. Nakazato, M. Takata and H. Nishihara, *J. Am. Chem. Soc.*, 2013, **135**, 2462–2465.
- A. J. Clough, J. W. Yoo, M. H. Mecklenburg and S. C. Marinescu, *J. Am. Chem. Soc.*, 2015, **137**, 118–121.
- D. L. Turner, T. P. Vaid, P. W. Stephens, K. H. Stone, A. G. DiPasquale and A. L. Rheingold, *J. Am. Chem. Soc.*, 2008, **130**, 14–15.
- X. Huang, H. Li, Z. Tu, L. Liu, X. Wu, J. Chen, Y. Liang, Y. Zou, Y. Yi, J. Sun, W. Xu and D. Zhu, *J. Am. Chem. Soc.*, 2018, **140**, 15153–15156.
- X. Huang, Y. Qiu, Y. Wang, L. Liu, X. Wu, Y. Liang, Y. Cui, Y. Sun, Y. Zou, J. Zhu, W. Fang, J. Sun, W. Xu and D. Zhu, *Angew. Chem., Int. Ed.*, 2020, **59**, 22602–22609.
- X. Huang, P. Sheng, Z. Tu, F. Zhang, J. Wang, H. Geng, Y. Zou, C. A. Di, Y. Yi, Y. Sun, W. Xu and D. Zhu, *Nat. Commun.*, 2015, **6**, 7408.
- T. Kambe, R. Sakamoto, T. Kusamoto, T. Pal, N. Fukui, K. Hoshiko, T. Shimojima, Z. Wang, T. Hirahara, K. Ishizaka, S. Hasegawa, F. Liu and H. Nishihara, *J. Am. Chem. Soc.*, 2014, **136**, 14357–14360.
- X. Huang, H. Yao, Y. Cui, W. Hao, J. Zhu, W. Xu and D. Zhu, *ACS Appl. Mater. Interfaces*, 2017, **9**, 40752–40759.
- Z. W. Jin, J. Yan, X. Huang, W. Xu, S. Y. Yang, D. B. Zhu and J. Z. Wang, *Nano Energy*, 2017, **40**, 376–381.
- Z. Wu, D. Adekoya, X. Huang, M. J. Kiefel, J. Xie, W. Xu, Q. Zhang, D. Zhu and S. Zhang, *ACS Nano*, 2020, **14**, 12016–12026.

- 19 H. Banda, J. H. Dou, T. Chen, N. J. Libretto, M. Chaudhary, G. M. Bernard, J. T. Miller, V. K. Michaelis and M. Dinca, *J. Am. Chem. Soc.*, 2021, **143**, 2285–2292.
- 20 X. Huang, S. Zhang, L. Liu, L. Yu, G. Chen, W. Xu and D. Zhu, *Angew. Chem., Int. Ed.*, 2018, **57**, 146–150.
- 21 T. Takenaka, K. Ishihara, M. Roppongi, Y. Miao, Y. Mizukami, T. Makita, J. Tsurumi, S. Watanabe, J. Takeya, M. Yamashita, K. Torizuka, Y. Uwatoko, T. Sasaki, X. Huang, W. Xu, D. Zhu, N. Su, J. G. Cheng, T. Shibauchi and K. Hashimoto, *Sci. Adv.*, 2021, **7**, eabf3996.
- 22 N. Arisnabarreta, P. Paredes-Olivera, F. P. Cometto and E. M. Patrio, *J. Phys. Chem. C*, 2019, **123**, 17283–17295.
- 23 L. Wu, Y. Jiao, K. Zhang, F. Wu, W. Zhao, M. Sun, A. Xie and W. Dong, *J. Mater. Chem. C*, 2019, **7**, 11621–11631.
- 24 O. Veselska and A. Demessence, *Coord. Chem. Rev.*, 2018, **355**, 240–270.
- 25 O. Veselska, L. Cai, D. Podbevsek, G. Ledoux, N. Guillou, G. Pilet, A. Fateeva and A. Demessence, *Inorg. Chem.*, 2018, **57**, 2736–2743.
- 26 Y. Cui, J. Yan, Z. Chen, J. Zhang, Y. Zou, Y. Sun, W. Xu and D. Zhu, *Adv. Sci.*, 2019, **6**, 1802235.
- 27 K. T. Butler, C. H. Hendon and A. Walsh, *ACS Appl. Mater. Interfaces*, 2014, **6**, 22044–22050.
- 28 E. A. Dolgoplova, A. J. Brandt, O. A. Ejegbavwo, A. S. Duke, T. D. Maddumapatabandi, R. P. Galhenage, B. W. Larson, O. G. Reid, S. C. Ammal, A. Heyden, M. Chandrashekhar, V. Stavila, D. A. Chen and N. B. Shustova, *J. Am. Chem. Soc.*, 2017, **139**, 5201–5209.
- 29 N. Massonnet, A. Carella, A. de Geyer, J. Faure-Vincent and J. P. Simonato, *Chem. Sci.*, 2015, **6**, 412–417.
- 30 J. F. Berry, F. A. Cotton, L. M. Daniels, C. A. Murillo and X. Wang, *Inorg. Chem.*, 2003, **42**, 2418–2427.
- 31 G. W. Cowell, A. Ledwith, A. C. White and H. J. Woods, *J. Chem. Soc. B*, 1970, 227–231.
- 32 J. J. Vittal, *Coord. Chem. Rev.*, 2007, **251**, 1781–1795.
- 33 G. K. Kole and J. J. Vittal, *Chem. Soc. Rev.*, 2013, **42**, 1755–1775.
- 34 T. H. Kim, Y. W. Shin, J. H. Jung, J. S. Kim and J. Kim, *Angew. Chem., Int. Ed.*, 2008, **47**, 685–688.
- 35 K. J. Lee, J. H. Lee, S. Jeoung and H. R. Moon, *Acc. Chem. Res.*, 2017, **50**, 2684–2692.